Mesoscopic atomic entanglement for precision measurements beyond the standard quantum limit

J. Appel, P. J. Windpassinger, D. Oblak, U. B. Hoff, N. Kjærgaard, and E. S. Polzik[1]

Danish National Research Foundation Center for Quantum Optics, The Niels Bohr Institute, University of Copenhagen, Blegdamsvej 17, DK-2100 Copenhagen Ø, Denmark

Edited by H. Jeffrey Kimble, California Institute of Technology, Pasadena, CA, and approved April 30, 2009 (received for review February 11, 2009)

Squeezing of quantum fluctuations by means of entanglement is a well-recognized goal in the field of quantum information science and precision measurements. In particular, squeezing the fluctuations via entanglement between 2-level atoms can improve the precision of sensing, clocks, metrology, and spectroscopy. Here, we demonstrate 3.4 dB of metrologically relevant squeezing and entanglement for $\gtrsim 10^5$ cold caesium atoms via a quantum nondemolition (QND) measurement on the atom clock levels. We show that there is an optimal degree of decoherence induced by the quantum measurement which maximizes the generated entanglement. A 2-color QND scheme used in this paper is shown to have a number of advantages for entanglement generation as compared with a single-color QND measurement.

spin squeezing | quantum nondemolition measurements | atomic clocks

When N_A independent 2-level atoms are prepared in an equal coherent superposition of the internal quantum states $|\uparrow\rangle$ and $|\downarrow\rangle$, a measurement of the ensemble population difference $\Delta N = N_\uparrow - N_\downarrow$ will fluctuate as $\sqrt{N_A}$ (see Fig. 1*A*). These fluctuations are referred to as projection noise (1, 2). More generally, the population difference of the ensemble can be shown to form 1 component of a collective pseudospin vector J. Taking $J_z = \frac{1}{2}\Delta N$, we have the variance $(\delta J_z)^2 = \frac{1}{4}N_A$ for the case of independent atoms also referred to as a coherent spin state (CSS). The CSS minimizes the Heisenberg uncertainty product so that, e.g., $(\delta J_z)^2(\delta J_x)^2 = \frac{1}{4}|\langle J_y\rangle|^2$ where $\langle J_y\rangle$ is the expectation value of the spin projection operator. At the expense of an increase in $(\delta J_x)^2$, it is possible to reduce $(\delta J_z)^2$ (or vice versa) below the projection noise limit while keeping their product constant. This constitutes an example of a spin squeezed state (SSS), for which the atoms need to be correlated. This correlation is ensured to be nonclassical if

$$(\delta J_z)^2 < \frac{|\langle J\rangle|^2}{N_A} \Rightarrow \xi \equiv \frac{(\delta J_z)^2}{|\langle J\rangle|^2}N_A < 1, \qquad [1]$$

where ξ defines the squeezing parameter. Under this condition, the atoms are entangled (3) and the prepared state improves the signal-to-noise ratio in spectroscopical and metrological applications (1).

Systems of 2 to 3 ions have successfully been used to demonstrate spectroscopic performance with reduced quantum noise and entanglement (4, 5). The situation is somewhat different with macroscopic atomic ensembles where spin squeezing has been an active area of research in the past decade (6–13). To our knowledge, no results reporting $\xi < 1$ via interatomic entanglement in such ensembles have been reported so far, with a very recent exception of the paper (14) where entanglement in an external motional degree of freedom of $2 \cdot 10^3$ atoms via interactions in a Bose–Einstein condensate is demonstrated.

Spin Squeezing by Quantum Nondemolition (QND) Measurements

In this article, we report on the generation of an SSS fulfilling Eq. **1** in an ensemble of $\approx 10^5$ atoms via a QND measurement (7, 15–17) of J_z. We show how to take advantage of the entanglement in this mesoscopic system by using Ramsey spectroscopy (1)—one of the methods of choice for precision measurements of time and frequency (18) (Fig. 1*A*). The figure presents the evolution of the pseudospin J whose tip is traveling over the Bloch sphere. The Ramsey method allows using the atomic ensemble as a sensor for external fields where the perturbation of the energy difference between the levels $\Delta E_{\uparrow\downarrow}$ is measured, or as a clock where the frequency of an oscillator is locked to the transition frequency between the two states $\Omega = \Delta E_{\uparrow\downarrow}/\hbar$. Fig. 1*B* illustrates how a suitable SSS can improve the precision of the Ramsey measurement provided that the condition of Eq. **1** is fulfilled.

Here we experimentally demonstrate 2 crucial steps of the entanglement-assisted Ramsey spectroscopy. First, we perform the projection noise squeezing (Fig. 1*C*) by a QND measurement. Second, by using the Ramsey method we measure the loss of atomic coherence $|\langle J\rangle|$ due to QND probing. Together, these results allow us to demonstrate the condition of Eq. **1**. The complete Ramsey sequence can be achieved if these 2 steps are supplemented with the rotation of the squeezed ellipse from the equatorial to the meridian plane (see Fig. S1 in the *SI Appendix*). We pay particular attention to a reliable determination of the projection noise level, which is an experimental challenge in its own right. A QND measurement based on far-off resonant dispersive probing is always accompanied by inherent decoherence due to spontaneous emission (shortening of $|\langle J\rangle|$, as in Fig. 1*B* and *C*) which affects entanglement according to Eq. **1**. As we show in the paper, the ensemble optical depth sets the optimal value of the decoherence, which has to be chosen in order to maximize the generated entanglement. We employ a dichromatic QND measurement (19) and show that it has several advantages for the SSS generation (20).

Experimental Setup. Cold Cs atoms are loaded into a far-off resonant optical dipole trap (FORT), aligned to overlap with the probe arm of a Mach-Zehnder-Interferometer (MZI, shown in Fig. 2*A*). The FORT is formed by a Gaussian laser beam with a wavelength of 1032 nm and a power of 2.5 W focused to a waist of 50 μm inside an evacuated glass cell located in one of the arms of the MZI (21, 22). Atoms are loaded into the FORT from a standard magnetooptical trap (MOT) superimposed onto the FORT, which collects and cools atoms from the background vapor to $\approx 50\,\mu$K. After loading the FORT, the MOT light is extinguished and a B-field of ~ 2 Gauss is applied, defining a quantization axis orthogonal to the trapping beam. At this stage, the atoms occupy the $(F = 4)$ ground level but are distributed amongst the magnetic sublevels. To polarize the atoms in one of the clock states, a combination of π-polarized laser light resonant to the $6S_{1/2}(F = 4) \rightarrow 6P_{3/2}(F' = 4)$

Author contributions: J.A., P.J.W., D.O., U.B.H., N.K., and E.S.P. designed research; J.A., P.J.W., D.O., U.B.H., N.K., and E.S.P. performed research; and J.A., N.K., and E.S.P. wrote the paper.

The authors declare no conflict of interest.

This article is a PNAS Direct Submission.

[1]To whom correspondence should be addressed. E-mail: polzik@nbi.dk.

This article contains supporting information online at www.pnas.org/cgi/content/full/0901550106/DCSupplemental.

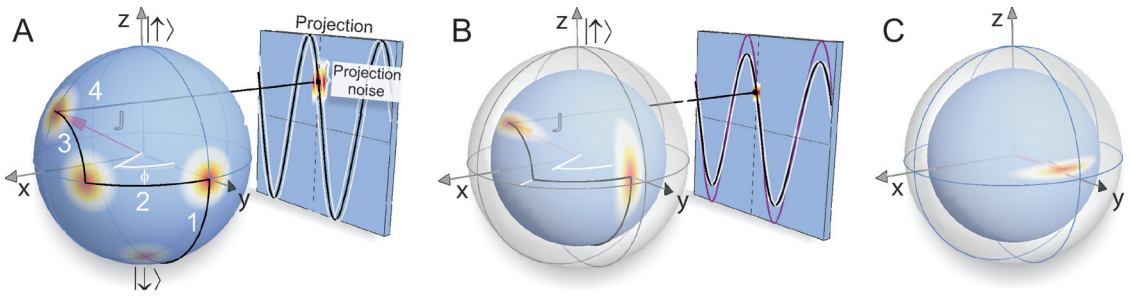

Fig. 1. Ramsey spectroscopy with coherent and squeezed states. (*A*) Bloch sphere representation of a Ramsey sequence with N_A atoms initially in the state $|\downarrow\rangle$ described by a Bloch vector $\langle J\rangle$ of length $N_A/2$ pointing toward the South Pole. Stage 1: A drive field of frequency ν near resonant to the $|\downarrow\rangle \leftrightarrow |\uparrow\rangle$ transition frequency ν_0 rotates the Bloch vector to the equator ($\pi/2$-pulse), bringing each atom into a superposition state $\frac{1}{\sqrt{2}}(|\uparrow\rangle + |\downarrow\rangle)$. This CSS is characterized by quantum fluctuations $(\delta J_z)^2 = (\delta J_x)^2 = \frac{1}{4}N_A$, illustrated as a fuzzy disk. Stage 2: The atoms evolve freely for a time T, and the Bloch vector precesses about the z axis by an angle $\phi = 2\pi(\nu - \nu_0)T$. ϕ is recorded after a second $\pi/2$-pulse (stage 3) by measuring the population difference (stage 4): $\cos\phi = (N_\uparrow - N_\downarrow)/N_A$. Projection noise will result in an uncertainty of the Ramsey fringe position. (*B*) The effect of projection noise in Ramsey spectroscopy can be reduced by applying an SSS. If the SSS is generated via a dispersive QND measurement, the accompanying spontaneous photon scattering leads to a fraction η of decohered atoms, thereby reducing the radius of the Bloch sphere and the Ramsey fringe amplitude by a factor $(1-\eta)$. Compared to the CSS shown in (*A*), the SSS on the reduced Bloch sphere (*B*) increases the precision in the determination of if the criteria Eq. **1** is fulfilled after the final $\pi/2$-pulse. (*C*) The present paper reports on the squeezing of $(\delta J_z)^2$, i.e. along the meridian direction, which can be converted into the squeezing in the equatorial direction by a microwave pulse. The SSS resides on a Bloch sphere of reduced radius as compared with the original CSS.

and $6S_{1/2}(F=3) \rightarrow 6P_{3/2}(F'=4)$ transitions is applied, optically pumping the atoms towards the $(F=4, m_F=0)$ state with 80% efficiency. Purification of clock state atoms proceeds by transferring the $(F=4, m_F=0)$ state atoms to the $(F=3, m_F=0)$ state using a resonant π-pulse on the clock transition and blowing away remaining atoms residing in the $(F=4)$ level with light on the $6S_{1/2}(F=4) \rightarrow 6P_{3/2}(F'=5)$ cycling transition. The CSS preparation is completed by putting the ensemble in an equal superposition of the clock states $\bigotimes_{i=1}^{N_A}[\frac{1}{\sqrt{2}}(|\downarrow\rangle + |\uparrow\rangle)]_i$ by applying a resonant $\pi/2$ microwave pulse at the clock frequency. Next, we perform successive QND measurements on the sample, after which all atoms are pumped into the $F=4$ level to determine the total atom number N_A. The sequence is repeated several thousand times for various N_A. A schematic representation of the experimental sequence is shown in Fig. 3*A*.

Measurement of the Projection Noise. The dispersive measurement of the clock state population difference (23, 24) is realized by detecting the state dependent phase shift of off-resonant probe laser light. In the present experiment, one probe $P_\downarrow$ is coupled to the state $|\downarrow\rangle \equiv 6S_{1/2}(F=3, m_F=0)$, while a second probe $P_\uparrow$ is coupled to the state $|\uparrow\rangle \equiv 6S_{1/2}(F=4, m_F=0)$ (see Fig. 2*B*).

Both probe beams enter the interferometer through different ports, so that the phase shifts imprinted on them by the atoms contribute with opposite signs to the differential signal Δn from the detectors D_1, D_2. As discussed below, this geometry, together with a suitable choice of probe detunings, provides compensation of a deleterious probe-induced shift of the measured frequency Ω. Denoting the sum photosignal as n, we define

$$\phi = \frac{\Delta n}{n} = \frac{\delta n}{n} + k_\uparrow N_\uparrow - k_\downarrow N_\downarrow, \qquad [2]$$

where $\delta n = \delta n_\uparrow + \delta n_\downarrow$ denotes the total shot noise contribution of both probe colors. The probes are of equal intensity and their detunings are chosen such that the coupling constants $k = k_\uparrow = k_\downarrow$ are equal. Hence, the normalized differential signal ϕ yields a J_z measurement with the optical shot noise added:

$$\phi = \frac{\delta n}{n} + k\Delta N = \frac{\delta n}{n} + 2kJ_z, \qquad [3]$$

$$\mathrm{var}(\phi) = \frac{1}{n} + k^2 \mathrm{var}(\Delta N). \qquad [4]$$

For atoms in a CSS, we have $\mathrm{var}(\Delta N) = N_A$ and Eq. **4** predicts a linear increase of the projectionnoise with the number of atoms.

Fig. 4 shows that we have observed the projection noise of atoms, as evidenced by the almost perfect linear fit to the noise data (blue points). To further confirm that the linear part of Fig. 4 is the quantum projection noise, we verify the value of k^2 for the inferred projection noise slope by independent means (see *SI Appendix*). Achieving this linearity is a demanding experimental task because it requires technical noise, e.g., fluctuations of the probe power and the interferometer length to affect ΔN measurements well below the level of $1/\sqrt{N_A} \approx 2 \cdot 10^{-3}$ over the time scale of the experiment.

Conditional Noise Reduction by QND Measurement. The ability to measure the atomic spin projection with a sensitivity limited by the shot noise of light allows us to produce a conditionally spin squeezed atomic state. After preparation of a CSS, we use n_1 photons to measure J_z as outlined above and obtain a measurement result ϕ_1, which is randomly distributed around zero with a variance $\frac{1}{n_1} + k^2 N_A$ (see Eq. **4**, blue dots in Fig. 4). By using the information obtained in the first measurement we can, to a certain degree, predict the outcome ϕ_2 of a successive J_z measurement performed on the same ensemble of atoms. The best estimate for ϕ_2 is $\zeta\phi_1$, which results in a conditionally reduced variance,

$$\mathrm{var}(\phi_2 - \zeta\phi_1) = \frac{1}{n_2} + \frac{1}{1+\kappa^2}k^2 N_A, \qquad [5]$$

that displays a reduction of the projection noise by $\frac{1}{1+\kappa^2}$ (see red diamonds in Fig. 4). The measurement strength $\kappa^2 = n_1 k^2 N_A$ describes the ratio of the atomic noise to the shot noise of light and $\zeta = \mathrm{cov}(\phi_1, \phi_2)/\mathrm{var}(\phi_1) = \kappa^2/(1+\kappa^2)$. A QND measurement with a finite strength κ^2 leads to finite correlation between the 2 measurements, as shown in Fig. 3*B*. For $\kappa^2 = 3.2$, observed for $N_A = 1.2 \cdot 10^5$ atoms, we expect a conditionally reduced variance of -6.2 dB with respect to the projection noise level. In the experiment, we find the value $-(5.3 \pm 0.7)$ dB as shown in Fig. 4.

Decoherence. Spontaneous emission caused by the QND probes is a fundamental, irreversible decoherence mechanism which affects the SSS in 2 ways. First, it can change the value of J_z by redistributing atomic populations via inelastic Raman scattering. This effect would be particularly important if a single QND probe coupled to both clock levels were used. Except for special cases such as discussed in (25), the single color probing causes Raman scattering between the clock levels. With the 2-color QND scheme we use here, the population redistribution between the hyperfine levels

PHYSICS

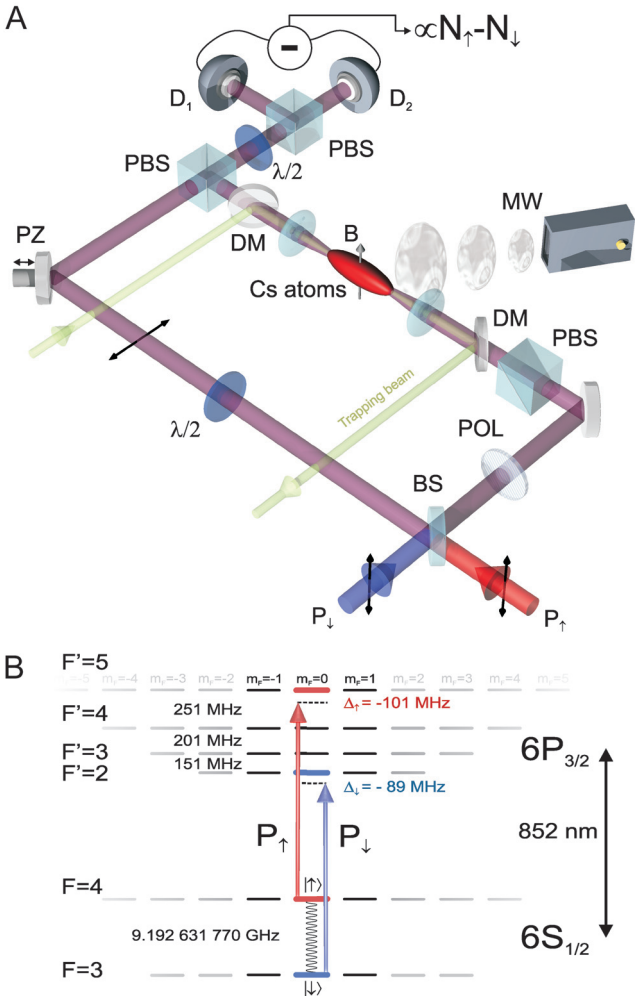

Fig. 2. Experimental setup. (*A*) An ensemble of $\sim 10^5$ Cs atoms cooled to $\approx$50 μK are confined in 1 arm of a MZI by a trapping beam with the waist of 50 μm folded by 2 dichroic mirrors (DM). The atoms are prepared in a coherent superposition of the clock states $|\uparrow\rangle$ and $|\downarrow\rangle$ by applying a microwave (MW) $\pi/2$-pulse. Two linearly polarized probe beams $P_\uparrow$ and $P_\downarrow$ enter the interferometer via separate ports of the input beam splitter (BS). The probes focused to the waist of 27 μm acquire phase shifts proportional to the number of atoms in the clock states $N_\uparrow$ and $N_\downarrow$, respectively. An arrangement of polarizers (POL), polarizing beam splitters (PBS), and half wave plates ($\lambda/2$) is used to adjust the powers and polarizations of the probe and reference beams. The combined phase shift ($\propto (N_\uparrow - N_\downarrow)$) of the 2 probes is measured in a balanced homodyne configuration. (*B*) Simplified level scheme of Cs showing the D2 line and the detunings of the clock state-sensitive probes, $P_\uparrow$ and $P_\downarrow$.

is practically absent because of the selection rules and the choice of detunings (atoms in the ground state level $F = 4$ are predominantly excited to the level $F' = 5$ and hence cannot decay to the ground state $F = 3$, and similarly for the reverse scattering). The effect of the redistribution between the magnetic sublevels within a given hyperfine level on the projection noise squeezing is very small (estimated to be less than 1%), as also proven by a good agreement between the observed and predicted degree of this squeezing (see *Dichromatic QND* and the *SI Appendix* for further discussion of this issue).

The second and main effect of the spontaneous decoherence on entanglement is due to the reduction of the coherence between the clock levels. Both inelastic Raman and elastic Rayleigh spontaneously scattered photons lead to shortening of the mean collective spin vector $|\langle J\rangle| \rightarrow (1-\eta)|\langle J\rangle|$ and hence to the reduction in Ramsey fringe amplitude (see Fig. 1*B*). The degree of spin squeezing as defined by Eq. **1** depends on the fraction η of atoms

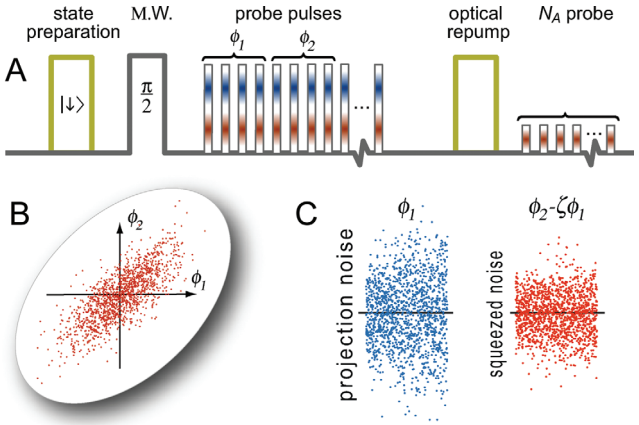

Fig. 3. Pulse sequence and noise data. (*A*) Atoms are prepared in state $|\downarrow\rangle$ by an optical pumping sequence and then rotated to the superposition state $\frac{1}{\sqrt{2}}(|\uparrow\rangle + |\downarrow\rangle)$ by a microwave $\pi/2$ pulse before the train of 10 probe pulses is applied. Combining the results of several pulses, we can change the effective QND measurement strength as explained in the text. The first effective probe pulse measurement result ϕ_1 yields the statistics of the J_z for the CSS. The second effective pulse measurement result ϕ_2 verifies the squeezing, provided it is sufficiently correlated with ϕ_1. N_A is measured at the end of each sequence. (*B*) Correlations between the first and the second pulse measurements. (*C*) The projection noise manifested in the random scattering of about 2,000 measurements of ϕ_1; and the SSS displayed as the reduced noise in ϕ_2 when the QND result is used as $(\phi_2 - \zeta\phi_1)$.

which decohere as a result of spontaneous photon scattering during dispersive QND probing. The QND measurement strength can be cast as $\kappa^2 \propto d\eta$ where d is the resonant optical depth of the sample (26). This highlights the trade-off between information gained

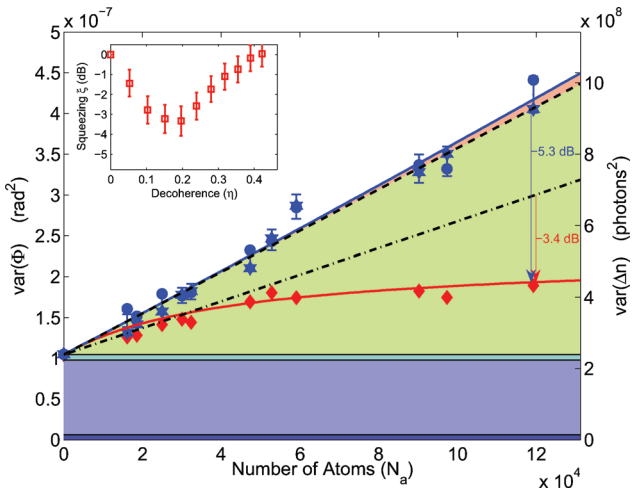

Fig. 4. Projection noise and spin squeezing. Blue points, stars; variances var(ϕ_1), var(ϕ_2) of the J_z spin noise measurement of atoms in a CSS versus N_A, error bars, corresponding statistical uncertainty centered on 1/2[var(ϕ_1) + var(ϕ_2)]; solid blue line, quadratic fit (see *Methods* section); dashed line, CSS projection noise; dash-dotted line, equivalent CSS projection noise reduced by the loss of atomic coherence; red diamonds, conditionally reduced variance of a second *Jz* spin measurement predicted by the first variance $(\phi_2 - \zeta\phi_1)$; red line, reduced noise of SSS predicted from quadratic fits to projection noise data (see *Methods* section); According to the scaling behavior, we classify different noise contributions (see *Data Analysis*). Classical fluctuations are represented by the cyan (empty interferometer) and red area (atom-light interaction related). Blue area, optical shot noise (light blue) and detector noise (dark blue); green area, projection noise. (*Inset*) Spin squeezing ξ (red boxes) as a function of the decoherence parameter η corresponding to the fits (dash-dotted black and red line in the main figure) evaluated for the atom number of the rightmost bin. Error bars, standard deviation over analysis runs binning into 5 to 30 groups with respect to N_a.

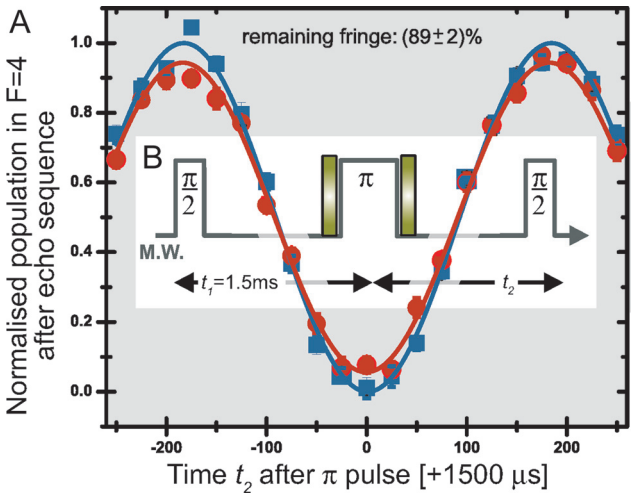

Fig. 5. Decoherence measurement. (*A*) Sample traces of the $F = 4$ population as function of the second $\pi/2$-pulse delay t_2. Blue squares serve as reference level for the fringe amplitude without any probe light pulses. Red points were obtained with a combined photon number in the 2 pulses of $2n_p = 7.4 \cdot 10^6$. From the fitted curves, the reduction of the fringe amplitude is inferred, giving an upper bound of $\eta = (0.11 \pm 0.02)$. (*B*) Experimental sequence similar to that of Fig 1*A* with the addition of a microwave π-pulse to reverse dephasing. Without the probe light pulses, the microwave $(\pi/2, \pi, \pi/2)$-pulse sequence compensates all reversible dephasing effects. Absorption of light from the 2 probe pulses causes a fraction η of atoms to undergo (irreversible) spontaneous emission.

through strong coupling and coherence lost due to spontaneous emission.

An inhomogeneous AC Stark shift due to the transverse intensity profile of the probe beam can, in principle, cause an additional dephasing and decoherence. However, as discussed in the section on dichromatic QND, this deleterious effect is strongly suppressed in our QND sequence.

We determine η via the reduction in the Ramsey fringe amplitude in a separate echo spectroscopy experiment (21, 22). The technique and results are summarized in Fig. 5. The reduction in echo fringe amplitude as a result of the probe light thus provides an upper bound for the decoherence inflicted.

Squeezing and Entanglement. The noise measurement data presented in Fig. 4 corresponds to $\eta = 20\%$ as measured in echo spectroscopy. According to Eq. **1** metrologically relevant spin squeezing and entanglement $\xi < 1$ for a given N_A can be claimed if the conditionally reduced variance of the verification measurement (red diamonds in Fig. 4) is less than the projection noise scaled down by the factor $(1 - \eta)^2$ (dash-dotted line in Fig. 4). In the inset of Fig. 4, we consider the maximum N_A-bin of the data and plot ξ versus η, varying the probe photon number by combining consecutive probe pulses (see *Methods* for details of the data analysis). Maximum squeezing $\xi = -(3.4 \pm 0.7)$ dB is observed with $\eta = 20\%$, corresponding to probing the atoms with $1.3 \cdot 10^7$ photons. The squeezing reduces as η increases further, confirming the notion that though a stronger measurement enables more precise estimation of J_z, this reduction in spin noise eventually ceases to be spectroscopically relevant as a result of decoherence.

Dichromatic QND. A single probe introduces a phase shift of the Ramsey fringe of $\approx$0.8 radians due to the Stark shift. If 2 properly balanced probes $P_\downarrow$ and $P_\uparrow$ have the same spatial mode the differential AC Stark shift of the clock states $|\downarrow\rangle$ and $|\uparrow\rangle$ is strongly suppressed, and the phase shift of the Ramsey fringe is reduced below the measurement precision. However, even in the presence of inevitable probe fluctuations which lead to a differential Stark shift, this shift does not affect the QND Ramsey sequence. The differential Stark shift caused by the misbalance of the 2 probes would affect the initial value of J_x—that is, it would add noise to the anti-squeezed component of the spin without affecting the squeezed component. J_x is not measured in the Ramsey sequence (see Eq. **S8** in the *SI Appendix*), and therefore the dichromatic QND method does not lead to a differential light shift of the clock transition (20). This feature is most important for both the precision and the accuracy in metrological applications.

Another advantage of the 2-color probing is due to the fact that, as opposed to the single probe QND schemes (23) where detuning is fixed roughly in the middle between the atomic levels of interest, the detuning of 2 probes can be adjusted. The detuning is then chosen so that the optimal value of the parameter η is obtained for a photon number around 10^7, a convenient value that minimizes the combined effect of the laser intensity and frequency classical fluctuations. At the same time, for a single probe QND the photon number corresponding to the optimal η would be approximately 10^{10}, thus demanding a challenging level of stabilization of the probe power to much better than 10^{-5}.

Finally, we discuss the fundamental advantage of a dichromatic QND measurement with cyclic transitions (20). Such probing does not add any noise to δJ_z^2. Hence, from Eq. **1** together with the theoretical estimate for δJ_z^2 after the QND measurement, an optimal squeezing of $\xi_{\min} = \frac{9}{4}\frac{1}{1+\kappa^2} \propto \frac{1}{d}$ is predicted for $\eta = \frac{1}{3}$, assuming a large resonant optical depth d. Note that the optimal experimental value of η as shown in the inset of Fig. 4 is close to, albeit somewhat smaller than, the theoretical optimum.

We emphasize that the theoretical scaling of $\xi_{\min} \propto d^{-1}$ for the dichromatic QND method using cyclic transitions is more favorable than the scaling $\xi_{\min} \propto d^{-1/2}$ for a conventional single-color QND scheme with cross-pumping (26).

The probe transitions used in the present paper are not exactly cyclic. The spontaneous emission does not reshuffle atoms between the hyperfine levels, but it does cause Raman scattering $m_F = 0 \rightarrow m_F = \pm 1$ within each hyperfine level. Atoms spontaneously scattered to both $m_F = 0$ and $m_F \neq 0$ do not add noise to the QND-assisted Ramsey sequence (see *SI Appendix* for details). The only additional partition noise of J_z (<1%), which appears after the spontaneous emission, is due to slightly different probe coupling to atoms $m_F = 0$ and $m_F \neq 0$. Interestingly, it becomes obvious from this discussion that the atoms which decohered to $m_F \neq 0$ states are part of the entangled state because, if they were removed after the QND measurement, the parameter ξ would grow due to the increased uncertainty of δJ_z^2.

Conclusion and Outlook. In summary, we have demonstrated a reduction of projection noise to $-(5.3 \pm 0.6)$ dB and metrologically relevant spin squeezing and entanglement of $-(3.4 \pm 0.7)$ dB on the Cs microwave clock transition. We analyze in detail the role of spontaneous photon scattering in the Ramsey sequence combined with QND measurements and demonstrate the optimal balance between decoherence and the measurement strength for generation of spin squeezing. The measurement precision improves with the number of atoms, hence it is important that we have demonstrated entanglement with the largest to-date number (over 10^5) of cold and trapped atoms. We show that the dichromatic QND measurement has several advantageous features in the clock and Ramsey spectroscopy settings.

The phase noise of our microwave reference (*HP8341B*) prevented us from a demonstration of the effect of the spin squeezing in a full clock cycle, even for integration times $<10^{-4}$ s. We expect to be able to improve on that with a better microwave source.

A crucial parameter defining the degree of spin squeezing generated with the QND method is the resonant optical depth of the atomic ensemble. Here we have shown that significant entanglement can be obtained with a modest optical depth of $\approx$16. The requirement of high optical depth poses a limitation on the applicability of our results to, e.g., projection noise-limited fountain

clocks (18) where the optical depth is usually kept around unity in order to avoid collisional shifts.

Spin squeezing is on the current agenda for optical clocks (27–29), which are affected by collisions to a much smaller extent. The first step along the lines discussed in the present paper in state-of-the-art lattice clocks has been demonstrated very recently in (30) where a nondestructive measurement using a Mach-Zehnder interferometer with sensitivity near the projection noise level has been reported. The dichromatic QND method can be particularly convenient in optical clocks if both clock levels are probed because the levels separated by optical energy can be probed with 2 independent lasers.

In systems with a low single-pass optical depth, the effective optical depth can be increased by utilizing an optical cavity as demonstrated recently (31) where results similar to ours have been obtained. Sensing and metrology for which a high optical depth and associated collisions are not a problem will probably be the main field of application for this method, unless the collisional shift itself is the goal of a Ramsey experiment (32).

Methods

Noise Measurement Sequence. The clock state-sensitive probes $P_\uparrow$ and $P_\downarrow$ enter the interferometer via opposite input ports (see Fig. 2) and are phase locked to achieve common mode rejection of frequency fluctuations when probing the atoms. Because of the opposite inputs, the differential output signal $D_2 - D_1$ for the empty interferometer has opposite signs for $P_\uparrow$ and $P_\downarrow$, and their intensity ratio is controlled as to achieve zero mean of the signal; hence the dichromatic interferometer becomes nearly insensitive to geometric length variations. With the intensity ratio fixed, the detunings of $P_\uparrow$ and $P_\downarrow$ are fine-tuned to achieve zero mean signal for atoms in the coherent superposition. The 2 probes are mode-matched, so that the transverse spatial distributions of $P_\uparrow$ and $P_\downarrow$ (waist size 27 μm) are very similar. Hence the differential AC Stark shift on the clock transition from a dichromatic probe pulse is significantly reduced across the entire atomic volume.

The geometric path length difference between the probe and reference arms of the interferometer is controlled by a piezo-actuated mirror. Prior to atomic probing, the mirror position is adjusted in a feedback loop to achieve zero differential interferometer output near the white light position using a sequence of weak auxiliary laser pulses at 840 nm. This light virtually does not interact with the atoms and provides a reference position from which the mirror is subsequently offset to obtain an individually balanced output for each of the 2 probe beams. This enables the strong rejection of the intensity noise in the probe pulses during superposition state measurements. The offset value depends on the (expected) number of trapped atoms. The atomic ensemble is probed at 20 μs intervals using a sequence of 20 dichromatic pulses with a duration of 10 μs and $n_{\rm pulse}$ photons per color, per pulse ($1.83\cdot10^6$ in the probe arm). The differential interferometer signal is sampled on a digital storage oscilloscope from which we determine the differential photon numbers $\{p_1, p_2 \ldots p_{20}\}$. After probing the superposition state, the interferometer is reset to its reference position, and the atoms are optically pumped into the $(F = 4)$ level to determine N_A. The trapped atoms are recycled for additional measurements by using optical pumping and purification (as described above) to reinitialize the ensemble. During each MOT cycle, 4 ensembles are interrogated and, additionally, 3 reference measurements without atoms are recorded.

Data Analysis. We combine up to $P = 10$ successive pulses, which allows us to vary the effective QND probe photon number $n = 2Pn_{\rm pulse}$, and obtain the phase shifts $\phi_1 = (p_1 + \cdots p_P)/n$, $\phi_2 = (p_{P+1} + \cdots + p_{2P})/n$. These measurements are sorted and grouped according to the atom number N_A. We fit a general quadratic function $V(N_A) = v_0 + v_1 N_A + v_2 N_A^2$ (solid blue line in Fig. 4) to var (ϕ_1) and var (ϕ_2) (blue points and stars) and another function $C(N_A) = c_0 + c_1 N_A + c_2 N_A^2$ to cov (ϕ_1, ϕ_2) to identify the light noise contribution $v_0 - |c_0| - d_0$ (light blue area), d_0 = detector noise (dark blue area), and the projection noise $v_1 N_A$ (green field, dashed line). Knowing the outcome of a ϕ_1 measurement, the best prediction for the successive ϕ_2 measurement on the same sample is $\zeta\phi_1$, with $\zeta = \text{cov}\,(\phi_1, \phi_2)/\text{var}\,(\phi_1)$. The conditionally reduced variance var $(\phi_2 - \zeta\phi_1)$ (red diamonds) is predicted by $R(N) = V(N)t(1 - (\frac{C(N)}{V(N)})^2)$ (red line). From a spin-echo measurement with pulses of $n_{\rm se} = 7.4 \cdot 10^6$, photons altogether resulting in a fringe contrast reduction of $\eta_{\rm se} = 11\%$ the value of spin squeezing for a QND measurement employing a total of $n_{\rm Probe}$ photons in the probe arm is then calculated as $\text{SQ} = 10\log_{10}(\frac{R(N_{A,\max}) - R(0)}{v_1 N_{A,\max}}(1 - \eta_{\rm se})^{-2n_{\rm Probe}/n_{\rm se}})$. To compensate for slow drifts in our setup, from each set of raw data $p_1 \ldots p_{20}$ we subtract the individual pulse data recorded in the previous MOT cycle and perform our data analysis on the differential values.

Decoherence Measurement. In Fig. 5 we show the decoherence measurements for 2 dichromatic probe light pulses containing in total $7.4 \cdot 10^6$ photons. The data has been taken at a microwave detuning of $\Delta\Omega = 3$ kHz from the clock transition frequency and the inversion of the phase through the microwave π-pulse was induced after 1.5 ms of free evolution. The 2 light pulses reduce the echo-fringe by $11 \pm 2\%$, and thus this forms an upper bound for η for the combined effect of these probe pulses. From this, we can deduce the decoherence η corresponding to a probe pulse with a photon number n_P as $\eta(n_P) \approx 1 - (1 - 0.11)^{\frac{n_P}{7.4\cdot10^6}}$.

We have also verified that the dichromatic probing employed in the QND measurement indeed provides a significant reduction of the differential Stark shift by measuring the fringe visibility reduction in the absence of the π-pulse. In cases when the 2 probes were mode-matched to better than 97%, we indeed observed an identical fringe reduction irrespectively of the π-pulse.

Appendix: Derivation of the QND Measurement Equation

To describe the propagation of the probe light through the atomic gas, we express its complex valued susceptibility by

$$\chi = \frac{n_A}{L}\frac{\lambda}{2\pi}Q, \quad Q = -\frac{3\lambda^2}{4\pi}\sum_l \frac{\wp_l}{\Delta_l/\gamma + i/2}, \qquad [6]$$

where for each probe color the sum is taken over all possible transitions; $\wp_l$ denote Clebsch–Gordan coefficients, Δ_l is the detuning from resonance, n_A is the atom column density, L is the interaction length, λ is the vacuum wavelength, and $1/\gamma$ the excited state lifetime.

Since the $P_\uparrow$ $(P_\downarrow)$ probe only interacts with atoms in the $|\uparrow\rangle$ $(|\downarrow\rangle)$ state, we can calculate the phase shift θ and absorption $e^{-\alpha}$ for a plane wave of the probe light passing through the cloud as follows:

$$\theta_{\uparrow,\downarrow} = \frac{1}{2}\text{Re}\,\frac{2\pi}{\lambda}L\chi_{\uparrow,\downarrow} = \frac{1}{2}n_{A\uparrow,\downarrow}\text{Re}\,Q_{\uparrow,\downarrow}, \qquad [7]$$

$$\alpha_{\uparrow,\downarrow} = \text{Im}\,\frac{2\pi}{\lambda}L\chi_{\uparrow,\downarrow} = n_{A\uparrow,\downarrow}\text{Im}\,Q_{\uparrow,\downarrow}. \qquad [8]$$

The Gaussian spatial profiles of the 2 probes $I_P(r) = \frac{2}{\pi w^2}e^{-2\frac{r^2}{w^2}}$ with a waist size $w = 27\,\mu$m are mode-matched to better than 97% by maximizing the interference fringe between the 2 spatial modes by using the same laser as input. The atomic cloud is laser-cooled and trapped in a far-detuned dipole trap, as described in detail in ref. 21, so that the transverse size of the cloud is about a factor of 2 larger than the probe cross-section; hence the total

column density n_A is considered constant across the probe cross section.

n_A can be expressed as the sum of the column densities of the individual states:

$$n_A = n_{A\uparrow}(r,\vartheta) + n_{A\downarrow}(r,\vartheta) \quad [9]$$

Due to quantum fluctuations in the difference of the populations in the $|\uparrow\rangle$ and $|\downarrow\rangle$ states, the individual contributions $n_{A\uparrow,\downarrow}(r,\vartheta)$ can differ for different positions (r,ϑ) within the beam.

The measurement of the probe phase shift is performed by interference with a mode-matched reference beam, and hence the differential number of photons measured by the detectors D_1, D_2 is given by

$$\Delta n_{\uparrow,\downarrow} = \pm 2\sqrt{t n_{R\uparrow,\downarrow} n_{P\uparrow,\downarrow}}\theta_{\uparrow,\downarrow}, \quad [10]$$

where

$$\theta_{\uparrow,\downarrow} = \frac{1}{2}\mathrm{Re}\, Q_{\uparrow,\downarrow}\int_0^{2\pi}\int_0^{\infty} \mathrm{d}\vartheta r\mathrm{d}r\, I(r) n_{A\uparrow,\downarrow}(r,\vartheta) \quad [11]$$

is the spatially averaged phase shift of the probe(s), $t = 63\%$ is the probability of the homodyne detection of a photon that has interacted with the clock atoms, n_R is the number of detected photons from the reference arm of the interferometer, n_P is the number of probe photons interacting with atoms, and $n_{A\uparrow,\downarrow}$ is the column density of the atomic cloud in the 2 clock states, respectively. Because the probes are injected via opposite input ports, the detector signals have opposite signs. In deriving Eq. **11**, we assumed that the phase shifts $\theta_{\uparrow,\downarrow}$ are small, such that $\sin(\theta_{\uparrow,\downarrow}) \approx \theta_{\uparrow,\downarrow}$.

The photon numbers for both probes are matched ($n_R \equiv n_{R\uparrow} = n_{R\downarrow}$, $n_P \equiv n_{P\uparrow} = n_{P\downarrow}$), whereas the detunings are chosen such that the differential number of photoelectrons (the signal) for the 2 probes is zero for equal populations of the clock levels, i.e., $\mathrm{Re}\, Q_\uparrow = \mathrm{Re}\, Q_\downarrow$. Hence with $\tilde{n} \equiv \sqrt{t n_R n_P} Q$ denoting the interferometer fringe amplitude, the total signal due to atoms can be expressed as

$$\Delta n = \tilde{n}\left[\mathrm{Re}\, Q\int_0^{2\pi}\int_0^{\infty} \mathrm{d}\vartheta r\mathrm{d}r\, I_P(r)(n_{A\uparrow}(r,\vartheta) - n_{A\downarrow}(r,\vartheta))\right]. \quad [12]$$

When the atoms are prepared in one of the clock states, say state $|\uparrow\rangle$, the interferometer signal measures the total number of probed atoms $\Delta n_{|\uparrow\rangle} = n_{A\uparrow}\tilde{n}\mathrm{Re}\, Q$.

When the clock atoms are prepared in a coherent superposition of the states $|\uparrow\rangle$ and $|\downarrow\rangle$ (the CSS), the expectation value for the signal is zero: $\langle \Delta n_{\mathrm{CSS}}\rangle = 0$. Because the CSS is a product state, there is no correlation in the noise of $n_{A\uparrow} - n_{A\downarrow}$ at different positions within the beam, and therefore (omitting optical shot noise for the rest of this section):

$$\begin{aligned}
&\mathrm{var}\,(\Delta n_{\mathrm{CSS}}) \\
&= \tilde{n}^2(\mathrm{Re}\, Q)^2 \mathrm{var}\left[\int_0^{2\pi}\int_0^{\infty} \mathrm{d}\vartheta r\mathrm{d}r\, I_P(r) n_{A\uparrow}(r,\vartheta) - n_{A\downarrow}(r,\vartheta)\right] \\
&= \tilde{n}^2(\mathrm{Re}\, Q)^2 \int_0^{2\pi}\int_0^{\infty} \mathrm{d}\vartheta r\mathrm{d}r (I_P(r))^2 \mathrm{var}\,[n_{A\uparrow}(r,\vartheta) - n_{A\downarrow}(r,\vartheta)] \\
&= \tilde{n}^2(\mathrm{Re}\, Q)^2 \frac{n_A}{\pi w^2}. \quad [13]
\end{aligned}$$

This motivates the definitions

$$\begin{aligned}
N_{\uparrow,\downarrow} &\equiv \int_0^{2\pi}\int_0^{\infty} \mathrm{d}\vartheta r\mathrm{d}r\, I_P(r)\pi w^2 n_{A\uparrow}(r,\vartheta), \\
N_A &\equiv \pi w^2 n_A, \quad n \equiv 2(n_R + t n_P), \quad k \equiv \frac{\tilde{n}\mathrm{Re}\, Q}{n\pi w^2} \quad [14]
\end{aligned}$$

so that from Eq. **12** we can derive Eq. **3**: $\phi = \frac{\Delta n}{n} = k\Delta N$. We find consistently that for all atoms in the state $|\uparrow\rangle$: $\phi_{|\uparrow\rangle} = kN_\uparrow = kN_A$ and for the CSS: $\langle \phi_{\mathrm{CSS}}\rangle = 0$, $\mathrm{var}\,(\phi_{\mathrm{CSS}}) = k^2\mathrm{var}\,(\Delta N) = k^2 N_A$.

ACKNOWLEDGMENTS. We thank R. Le Targat and J.H. Müller for helpful discussions. This work was funded by the Danish National Research Foundation and European Union Grants COMPAS, EMALI, and QAP. N.K. was supported by a Danish Natural Science Research Council Steno fellowship.

1. Wineland DJ, Bollinger JJ, Itano WM, Moore FL, Heinzen DJ (1992) Spin squeezing and reduced quantum noise in spectroscopy. *Phys Rev A* 46:R6797–R6800.
2. Kitagawa M, Ueda M (1993) Squeezed spin states. *Phys Rev A* 47:5138–5143.
3. Sørensen A, Duan LM, Cirac JI, Zoller P (2001) Many-particle entanglement with Bose-Einstein condensates. *Nature* 409:63–66.
4. Leibfried D, et al. (2004) Toward Heisenberg-limited spectroscopy with multiparticle entangled states. *Science* 304:1476–1478.
5. Roos CF, Chwalla M, Kim K, Riebe M, Blatt R (2006) 'Designer atoms' for quantum metrology. *Nature* 443:316–319.
6. Hald J, Sørensen JL, Schori C, Polzik ES (1999) Spin squeezed atoms: A macroscopic entangled ensemble created by light. *Phys Rev Lett* 83:1319–1322.
7. Kuzmich A, Mandel L, Bigelow NP (2000) Generation of spin squeezing via continuous quantum nondemolition measurement. *Phys Rev Lett* 85:1594–1597.
8. Orzel C, Tuchman AK, Fenselau ML, Yasuda M, Kasevich MA (2001) Squeezed states in a bose-einstein condensate. *Science* 291:2386–2389.
9. Sørensen A, Mølmer K (2001) Entanglement and extreme spin squeezing. *Phys Rev Lett* 86:4431–4434.
10. Andre A, Sørensen A, Lukin M (2004) Stability of atomic clocks based on entangled atoms. *Phys Rev Lett* 92:230801.
11. Gerbier F, Fölling S, Widera A, Mandel O, Bloch I (2006) Probing number squeezing of ultracold atoms across the superfluid-Mott insulator transition. *Phys Rev Lett* 96:090401.
12. Fernholz T, et al. (2008) Spin squeezing of atomic ensembles via nuclear-electronic spin entanglement. *Phys Rev Lett* 101:073601.
13. Takano T, et al. (2009) Spin squeezing of a cold atomic ensemble with the nuclear spin of one-half. *Phys Rev Lett* 102:033601.
14. Estève J, Gross C, Weller A, Giovanazzi S, Oberthaler MK (2008) Squeezing and entanglement in a Bose-Einstein condensate. *Nature* 455:1216–1219.
15. Guerlin C, et al. (2007) Progressive field-state collapse and quantum non-demolition photon counting. *Nature* 448:889–893.
16. Caves CM, Thorne KS, Drever RWP, Sandberg VD, Zimmermann M (1980) On the measurement of a weak classical force coupled to a quantum-mechanical oscillator. I. issues of principle. *Rev Mod Phys* 52:341–392.
17. Atature M, Dreiser J, Badolato A, Imamoglu A (2007) Observation of Faraday rotation from a single confined spin. *Nat Phys* 3:101–105.
18. Santarelli G, et al. (1999) Quantum projection noise in an atomic fountain: A high stability cesium frequency standard. *Phys Rev Lett* 82:4619–4622.
19. Kuzmich A, Bigelow NP, Mandel L (1998) Atomic quantum non-demolition measurements and squeezing. *Europhys Lett* 42:481–486.
20. Saffman M, Oblak D, Appel J, Polzik ES (2008) Spin squeezing of atomic ensembles by multi-color quantum non-demolition measurements. *Phys Rev A*, 10.1103/PhysRevA.79.023831.
21. Oblak D, et al. (2008) Echo spectroscopy of atomic dynamics in a gaussian trap via phase imprints. *Eur Phys J D* 50:67–73.
22. Windpassinger PJ, et al. (2008) Inhomogeneous light shift effects on atomic quantum state evolution in non-destructive measurements. *New J Phys* 10:053032.
23. Oblak D, et al. (2005) Quantum-noise-limited interferometric measurement of atomic noise: Towards spin squeezing on the Cs clock transition. *Phys Rev A* 71:043807.
24. Windpassinger PJ, et al. (2008) Nondestructive probing of rabi oscillations on the cesium clock transition near the standard quantum limit. *Phys Rev Lett* 100:103601.
25. Ozeri R, et al. (2005) Hyperfine coherence in the presence of spontaneous photon scattering. *Phys Rev Lett* 95:030403.
26. Hammerer K, Sørensen A, Polzik ES (2008) Quantum interface between light and atomic ensembles. arXiv:0807.3358 [quant-ph].
27. Meiser D, Ye J, Holland M (2008) Spin squeezing in optical lattice clocks via lattice-based QND measurements. *New J Phys*, 10.1088/1367-2630/10/7/073014.
28. Wilpers G, et al. (2002) Optical clock with ultracold neutral atoms. *Phys Rev Lett* 89:230801.
29. Ludlow AD, et al. (2008) Sr lattice clock at 10-16 fractional uncertainty by remote optical evaluation with a Ca clock. *Science* 319:1805–1808.
30. Lodewyck J, Westergaard PG, Lemonde P. (2009) Non-destructive measurement of the transition probability in a Sr optical lattice clock. arXiv:0902.2905 [quant-ph].
31. Schleier-Smith MH, Leroux ID, Vuletić V (2008) Reduced-quantum-uncertainty states for an atomic clock. arXiv:0810.2582 [quant-ph].
32. Hart RA, Xu X, Legere R, Gibble K (2007) A quantum scattering interferometer. *Nature* 446:892–895.